Preprints.org

Article

Not peer-reviewed version

Research on Electric Oil-Pneumatic Active Suspension Based on Fractional Order PID Position Control

Yaozeng Hu , Jianze Liu * , Zhuang Wang , Jingming Zhang , Jiang Liu

Posted Date: 17 January 2024

doi: 10.20944/preprints202401.1302.v1

Keywords: fractional order damping; oil-pneumatic actuator; fractional order PID control; particle swarm algorithm; active suspension

Preprints.org is a free multidiscipline platform providing preprint service that is dedicated to making early versions of research outputs permanently available and citable. Preprints posted at Preprints.org appear in Web of Science, Crossref, Google Scholar, Scilit, Europe PMC.

Copyright: This is an open access article distributed under the Creative Commons Attribution License which permits unrestricted use, distribution, and reproduction in any medium, provided the original work is properly cited.

Preprints (www.preprints.org) | NOT PEER-REVIEWED | Posted: 17 January 2024 doi:10.20944/preprints202401.1302.v1

Disclaimer/Publisher's Note: The statements, opinions, and data contained in all publications are solely those of the individual author(s) and contributor(s) and not of MDPI and/or the editor(s). MDPI and/or the editor(s) disclaim responsibility for any injury to people or property resulting from any ideas, methods, instructions, or products referred to in the content.

Article

Research on Electric Oil-Pneumatic Active Suspension Based on Fractional Order PID Position Control

Yaozeng Hu, Jianze Liu *, Wang Zhuang, Jingming Zhang and Jiang Liu

Institute of Mechanical and Automotive Engineering, Qingdao University of Technology, Qingdao 266520, China

* Correspondence: liujiang@qut.edu.cn; Tel.: +86-15866817346

Abstract: Due to the nonlinear stiffness and fractional-order damping characteristics of some real suspension systems, coupled with the presence of viscoelastic materials, fractional-order nonlinear suspension system modeling has become a focus of research in recent years. In this study, an electric oil and gas actuator based on fractional-order PID position feedback control is proposed, through which the damping coefficient of the suspension system is adjusted to realize the active control of the suspension. A fractional order PID algorithm is used to control the motor's rotational angle to realize the damping adjustment of the suspension system. In this process, the road roughness is collected by the sensors as the criterion of damping adjustment, and the particle swarm algorithm is utilized to find the optimal objective function under different road surface slopes, to obtain the optimal cornering value. According to the mathematical and physical model of the suspension system, the simulation model and the corresponding test platform of this type of suspension system are built. The simulation and experimental results show that the simulation results of the fractional-order nonlinear suspension model are closer to the actual experimental values than those of the traditional linear suspension model, and the accuracy of each performance index is improved by more than 18.5%. The designed active suspension system optimizes the body acceleration, suspension dynamic deflection, and tire dynamic load to 89.8%, 56.7%, and 73.4% of the passive suspension, respectively. Notably, the designed fractional order PID control circuit for the motor shows better control results compared to the conventional PID control circuit. This study provides an effective theoretical and empirical basis for the control and optimization of fractional-order nonlinear suspension systems.

Keywords: fractional order damping; oil-pneumatic actuator; fractional order PID control; particle swarm algorithm; active suspension

1. Introduction

As the automotive industry continues to progress, the need for smooth vehicle ride and handling stability is increasing. Research on semi-active and active suspensions has become a popular area of interest. However, despite the many excellent semi-active suspension and active suspension schemes proposed [1–4], the past research on suspension systems composed of linear damping and nonlinear stiffness is no longer applicable to the various suspension types that are widely used today, such as magnetorheological suspensions [5], air suspensions [6], and hydro-pneumatic suspensions [7].

Therefore, it is important to create a fractional-order nonlinear suspension system containing nonlinear stiffness and fractional-order damping and to optimize the parameters of the fractional-order damping coefficients of this system.

The primary problem facing the study of this type of suspension system is to transform the linear damping force in the suspension system into a fractional-order damping force. You, H [8] et al. tuned the suspension stiffness and damping by introducing two tuning values, and at the same time introduced a fractional-order damping force to simulate the viscoelastic properties of the material. They used a particle swarm algorithm to optimize these two adjustment values and initially established a fractional-order passive suspension system containing two degrees of freedom.

© 2024 by the author(s). Distributed under a Creative Commons CC BY license.

Preprints (www.preprints.org) | NOT PEER-REVIEWED | Posted: 17 January 2024 doi:10.20944/preprints202401.1302.v1

However, the elastic elements of this system still exhibit linear elastic forces and stiffness. On the other hand, Chang, YJ [9], et al. investigated the active control of a fractional order nonlinear suspension system. They designed a linearization method for the feedback of the suspension system based on the differential geometry method and obtained the optimal control rate through LQR control, which led to the optimization of the damping performance of the suspension system. However, the study only used simulation to verify the control effect. Therefore, to verify the optimization degree of the fractional-order nonlinear suspension model more comprehensively, this paper constructs a fractional-order nonlinear oil-air suspension isometric test bed. The optimization effect of the model is verified by comparing the simulation and experimental results.

In addition to the in-depth study of suspension system modeling, actuator structures, and control algorithms have become the core topics of interest in the field of active suspension. Currently, the widely adopted active suspension actuator structures include rotary motor type, linear motor type [10], and electric oil and gas type [11]. Among them, the rotary motor actuator covers different forms such as rack and pinion [12], crank linkage [13], and ball screw [14]. The electric oil and gas actuator designed in this paper is structurally similar to the electrostatic actuator. The electrostatic actuator is mainly composed of two parts: the mechanical module (including hydraulic cylinders, hydraulic pumps, and coil springs) and the electrical module (including power supply, controller, DC motor, and the corresponding signal detection device). The electric oil and gas actuator, on the other hand, transforms the hydraulic cylinder and hydraulic pump in the mechanical structure into an oil and gas damper with adjustable damping, and the rest of the structure remains similar. As we all know, compared with the hydraulic damper, the oil and gas damper is equipped with an air chamber at the bottom, which can skillfully use air pressure to alleviate the vibration, and thus theoretically has a more excellent damping effect. In the electric module, the algorithm used for DC motor control has been improved and shifted from the common PID control algorithm to the fractional order PID control algorithm, which was proposed by Podlubny [15]. Two additional control parameters λ and μ were introduced in the fractional order PID controller, where λ denotes the fractional order of the integral link I in the fractional order PID control, and μ denotes the fractional order of the differential link D in the fractional order PID control. This improvement allows for a wider and finer tuning range of the controller parameters, thus allowing for a more accurate determination of the strength of the proportional, integral, and differential links. This further improves the motor response speed and control accuracy, resulting in a more rapid and accurate damping adjustment of the oil and gas actuator.

In summary, this paper presents an electric hydrocarbon active suspension with fractional-order PID position control and describes a fractional-order nonlinear model of this suspension system. The accuracy of the simulation model of the fractional-order nonlinear suspension system, the feasibility of the designed actuator structure, and the excellent performance of the adopted fractional-order PID control algorithm are verified by comparing the simulation and experimental results.

2. Principle and Modeling

2.1. Electric oil-pneumatic active suspension working principle

The design of the electric oil-air active suspension used in this paper is mainly based on an oil-air damper with adjustable damping. The suspension system measures the acceleration of the vehicle through acceleration sensors and feeds the signal back to the controller. The controller manipulates the rotation angle of the DC motor through a control circuit, which in turn realizes the damping adjustment of the damper through a gearbox transmission. This process allows the actuator to output adjustable damping force, thus realizing active control of the suspension system. The workflow of the hydro-pneumatic active suspension is shown in Figure 1.

Preprints (www.preprints.org) | NOT PEER-REVIEWED | Posted: 17 January 2024 doi:10.20944/preprints202401.1302.v1

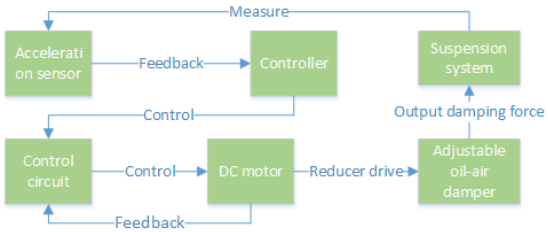

Figure 1. oil-pneumatic active suspension workflow.

2.2. Fractional order damping force model for the electric oil-pneumatic actuator

Since the characteristics of electric oil and gas actuators are affected by a variety of factors, including conditions such as excitation frequency, external temperature, and usage history, this is consistent with the mechanical properties of viscoelastic materials. And since viscoelastic materials have both viscous and elastic properties, it is more accurate and reasonable to use a fractional order calculus model [16] describing viscoelastic materials to depict the mechanical properties of the oil and gas damper. And the fractional-order damped Duffing system model [17] describing the viscoelastic characteristics of the material is referenced in the design of the oil and gas suspension model. The fractional-order damping force at the output of the actuator can be calculated by the following equation.

$$F_c = c_s \cdot D^p(x_2 - x_1), 0 < p < 1 \tag{1}$$

where x_2 is the spring-loaded mass displacement, x_1 is the unsprung mass displacement, p is the order of the fractional order differential term, and c_s is the fractional order viscoelastic damping coefficient of the suspension system. $D^p(.)$ is the fractional order calculus operator, and the three main definitions of fractional order calculus used so far are the Riesmann-liouville formula, Grunwald-Letnikov formula, and Caputo formula. In this paper, the Grunwald-Letnikov formula [18] is used to define the fractional order calculus operator, and its differential definition is shown in the following equation.

$${}^{GL}_{t_0}D_t^p f(t) = \lim_{h\to 0} \frac{1}{h^p} \sum_{j=0}^{[(t-t_0)/h]} (-1)^j \binom{p}{j} f(t - jh) \tag{2}$$

where $[(t\text{-}t_0)/h]$ means taking the nearest integer to $(t\text{-}t_0)/h$, $\binom{\alpha}{j}$ is the coefficient of the binomial; the definition of the integral only requires changing the fractional order p in the differential equation (2) to $-p$.

Since the damping of the oil-pneumatic actuator used is adjustable, the fractional order viscoelastic damping coefficient c_s and the actuator damping force F_c are calculated as shown in equations (3) and (4).

$$c_s = b \cdot c \tag{3}$$

$$F_c = b \cdot c \cdot D^p(x_2 - x_1), 0 < p < 1 \tag{4}$$

where b is the damping scale of adjustable dampers, $10 \geq b \geq 1$; c is the damping coefficient of the passive suspension.

2.3. Suspension system modeling

In this paper, a fractional-order nonlinear suspension system model is constructed mainly based on the viscoelastic properties of the employed adjustable-damped oil-air actuator. The constructed

Preprints (www.preprints.org) | NOT PEER-REVIEWED | Posted: 17 January 2024 doi:10.20944/preprints202401.1302.v1

active model of the 1/4 vehicle suspension system is shown in Figure 2 below. In this figure, F_k denotes the elastic force output from the nonlinear elastic element, m_2 represents the spring load mass, m_1 represents the unsprung load mass, k_1 is the tire stiffness, and q represents the road excitation.

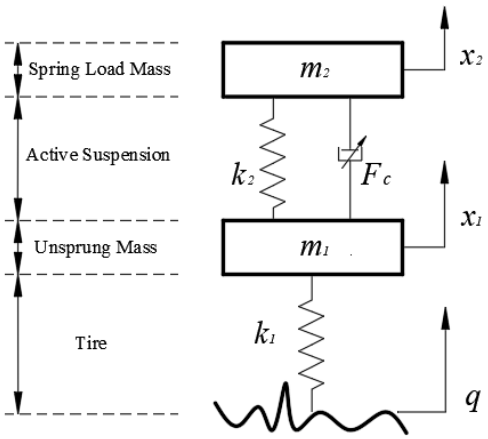

Figure 2. Fractional order nonlinear active suspension system.

The equation for the nonlinear elastic force F_k in the figure is shown in the following equation.

$$F_k = k_2(x_2 - x_1) + e(x_2 - x_1)^3 \tag{5}$$

where k_2 is the linear stiffness of the elastic element and e is the nonlinear coefficient of the elastic element.

From Figure 2 combined with equation (5), the differential equation of motion of the suspension system can be obtained as:

$$\begin{cases} m_2\ddot{x}_2 + k_2(x_2 - x_1) + e(x_2 - x_1)^3 \\ +b \cdot c \cdot D^p(x_2 - x_1) = 0 \\ m_1\ddot{x}_1 - k_2(x_2 - x_1) - e(x_2 - x_1)^3 \\ -b \cdot c \cdot D^p(x_2 - x_1) + k_1(x_1 - q) = 0 \end{cases} \tag{6}$$

In the study of the 1/4 suspension system, the conventional passive nonlinear suspension system model differential equation of motion is shown in the following equation.

$$\begin{cases} m_2\ddot{x}_2 + k_2(x_2 - x_1) + e(x_2 - x_1)^3 \\ +c \cdot (\dot{x}_2 - \dot{x}_1) = 0 \\ m_1\ddot{x}_1 - k_2(x_2 - x_1) - e(x_2 - x_1)^3 \\ -c \cdot (\dot{x}_2 - \dot{x}_1) + k_1(x_1 - q) = 0 \end{cases} \tag{7}$$

2.4. Pavement excitation model

A filtered white noise pavement model was used to construct the pavement input excitation q for the active control study process [19], with the following principle formula.

$$\dot{q}(t) = 2\pi n_0 \sqrt{G_0 v} \cdot w(t) - 2\pi f_0 q(t) \tag{8}$$

Preprints (www.preprints.org) | NOT PEER-REVIEWED | Posted: 17 January 2024 doi:10.20944/preprints202401.1302.v1

Where n_0 is the reference spatial frequency; G_0 is the road surface unevenness coefficient; f_0 is the space under the cut-off frequency; v is the vehicle speed of 50km/h. Since the amplitude range of the shaker in the experimental equipment is 0-0.01m, $w(t)$ is taken as 0.04 unit intensity of Gaussian white noise.

In this paper, regarding the parameters of the international standard ISO 8608 [20] for A, B, and C pavements, the three classes of pavements are combined to form the pavement excitation used in the study, and to consider only the effects caused by pavement unevenness, the pavement excitation formula is designed as shown in the following equation.

$$\dot{q}(t)=\begin{cases}2\pi n_0\sqrt{G_1 v}\cdot w(t)-2\pi f_0 q(t), 0\le t<5\\ 2\pi n_0\sqrt{G_2 v}\cdot w(t\text{-}3)-2\pi f_0 q(t\text{-}3), 5\le t<10\\ 2\pi n_0\sqrt{G_3 v}\cdot w(t\text{-}6)-2\pi f_0 q(t\text{-}6), 10\le t\le 15\end{cases} \quad (9)$$

G_1, G_2, and G_3 are the geometric means of pavement unevenness coefficients for A, B, and C-class pavements, respectively. The pavement excitation images are shown in Figure 3 below.

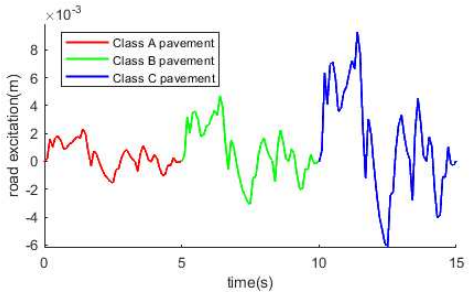

Figure 3. Pavement excitation model.

2.5. Electric oil-pneumatic actuator model

The oil and gas-electric actuator mainly consists of a DC motor, a worm gear reducer, and an oil and gas damper with adjustable damping. The reasons for connecting the worm gear reducer to the DC motor and the oil and gas damper are as follows:

1)Improvement of motor position control accuracy: Due to the small rotation angle of the motor shaft, its position control accuracy is relatively low. In addition, dampers usually require a smaller adjustment range. Therefore, installing a gear reducer helps to ensure high accuracy of motor position control.

2)Increased torque: In an isometric drive, the output torque of the motor may not be sufficient to drive the rotation of the damper adjustment knob. By installing a gear reducer, the output torque can be effectively increased to ensure proper operation of the damper.

3)Reduced Space Occupancy: The turbine worm gear reducer is smaller in size compared to the gear reducer, which helps to reduce the space occupied by the actuator and improve the compactness of the overall system.

The simple mechanical structure of an electric oil and gas actuator is shown in Figure 4.

Preprints (www.preprints.org) | NOT PEER-REVIEWED | Posted: 17 January 2024 doi:10.20944/preprints202401.1302.v1

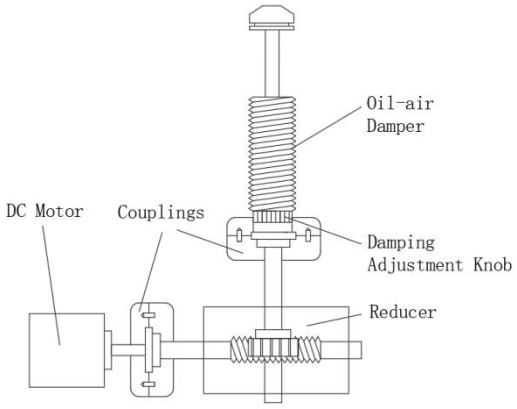

Figure 4. Mechanical structure diagram of the electric oil-pneumatic actuator.

Known worm gear reducer reduction ratio i, when the motor angle position is 0 (motor shaft rotation 0 rad), the scale parameter b=1 in equation (2). When the motor angular position reaches the maximum value of damping adjustment (when the motor shaft rotates $2\pi/i$ rad), the scale parameter b=10, from which the relationship between the motor shaft rotation angle θ and the parameter b can be obtained as shown in the following equation.

$$b = \frac{9i\theta + 2\pi}{2\pi} \tag{10}$$

The relationship between the output damping force of the damper and the rotation angle of the motor shaft can be obtained by combining (4) and (10):

$$F_c = (\frac{9i\theta + 2\pi}{2\pi}) \cdot c \cdot D^p (x_2 - x_1) \tag{11}$$

The above equation can be used to control the output damping force of the actuator by controlling the angle of rotation of the motor.

2.6. DC motor mathematical model

The equivalent circuit diagram of the DC motor is shown in Figure 5 below. In the figure, U represents the supply voltage, L is the motor inductance, I is the armature circuit current, r is the motor internal resistance, E_M is the motor-induced electric potential, ω is the motor shaft rotation angular velocity, and T is the motor output torque.

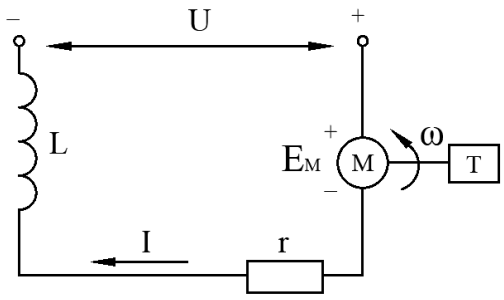

Figure 5. DC Motor Equivalent Circuit Diagram.

From Figure 5 above, the motor voltage balance equation can be obtained as shown in the following equation.

$$U = Ir + L\frac{dI}{dt} + E_M \tag{12}$$

Preprints (www.preprints.org) | NOT PEER-REVIEWED | Posted: 17 January 2024 doi:10.20944/preprints202401.1302.v1

where t is the time.

The equations of induction potential, electromagnetic torque, and torque balance of a DC motor are known as shown in equations (13), (14), and (15), respectively.

$$E_M = K_E \cdot \omega \tag{13}$$

$$T = K_T \cdot I \tag{14}$$

$$T = J\frac{d\omega}{dt} + T_d \tag{15}$$

Where K_E is the counter-electromotive force constant, K_T is the torque constant, J is the total rotational inertia of the working mechanical system converted to the motor shaft, and T_d is the load torque. It is known that the angular velocity of motor shaft rotation ω=dθ/dt, and the mathematical model equation of the DC motor can be obtained from the above equation (12), (13), (14), and (15).

$$\begin{cases} \dfrac{dI}{dt} = (U - Ir - K_M \cdot \dfrac{d\theta}{dt}) / L \\ \dfrac{d^2\theta}{dt^2} = (K_T \cdot I - T_d) / J \end{cases} \tag{16}$$

The Laplace transform of the above equation (16), due to the effect of the reducer, the load torque of the motor is very small and can be neglected here, and the result of the transformation is shown in the following equation.

$$\begin{cases} \mathrm{L} \cdot I(s) \cdot s = U(s) - I(s)r - K_M \cdot s \cdot \theta(s) \\ J \cdot s^2 \cdot \theta(s) = K_T \cdot I(s) \end{cases} \tag{17}$$

From the above equation, the transfer function $H(s)$ of the DC motor turning angle θ and the motor voltage U is given by the following equation.

$$H(s) = \frac{\theta(s)}{U(s)} = \frac{K_T}{JL \cdot s^3 + Jr \cdot s^2 + K_M K_T \cdot s} \tag{18}$$

3. Principle of active control of suspension system

In this study, the objective function of the suspension system is optimized by using the particle swarm algorithm so that the controller outputs the ideal rotation angle parameter of the motor, and the control principle is schematically shown in Figure 6. The particle swarm algorithm is used to optimize the simple harmonic excitation objective function J_1 with different frequencies and amplitudes to derive the parameter of the ideal rotation angle θ_0. The DC motor control circuit outputs the actual rotation angle θ according to the ideal rotation angle θ_0, and the oil-air damper adjusts the damping according to the actual rotation angle output by the motor, to realize the output of the damping force F_c to achieve a superior suspension control effect. In Figure 6, the working principle of the DC motor control circuit is mainly demonstrated in Figure 7. The current DC motor rotation angle θ forms a deviation value e_1 from the given rotation angle θ_0, and the output power supply voltage U is controlled by the fractional-order PID control algorithm, thus realizing the precise control of the DC motor rotation angle.

Preprints (www.preprints.org) | NOT PEER-REVIEWED | Posted: 17 January 2024 doi:10.20944/preprints202401.1302.v1

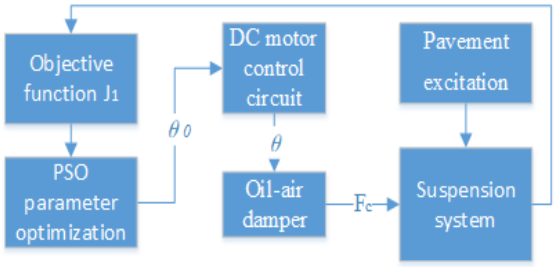

Figure 6. Control schematic of suspension system.

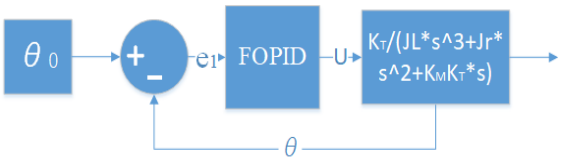

Figure 7. DC motor control circuit schematic.

3.1. Fractional order PID controller simulation design

The transfer function of the fractional order PID controller is shown in the following equation.

$$G(s) = K_p + K_i / s^{-\lambda} + K_d s^{\mu} \tag{19}$$

In this paper, a modified oustaloup filter [21] is used to implement the approximation of the fractional order calculus operator s^{α}. The main steps in constructing the fractional order calculus operator are as follows:

1)Determine the filter order N and the approximate frequency band [w_b, w_h].

2)Calculate the zero pole $w_k^{'}$ and w_k, which is calculated as shown in equations (20) and (21).

$$w_k^{'} = w_b w_{\mu}^{(2k-1-\alpha)/N}, w_k = w_b w_{\mu}^{(2k-1+\alpha)/N} \tag{20}$$

$$k = w_h^{\alpha}, w_{\mu} = \sqrt{w_h / w_b} \tag{21}$$

3)Finally, the approximation to the fractional order calculus operator is completed, as shown in equation (22).

$$s^{\alpha} = (\frac{dw_h}{b})^{\alpha} (\frac{ds^2 + bw_h s}{d(1-\alpha)s^2 + bw_h s + d\alpha}) \prod_{k=1}^{N} \frac{s + w_k^{'}}{s + w_k} \tag{22}$$

The above equation α must be satisfied ($0<\alpha<1$). In general, the approximate frequency band is set as [0.001,1000], the filter order N is 5, and the weighting parameters are selected as b=10, d=9 to meet the accuracy requirements. The improved oustaloup filter for $s^{-\lambda}$ and $s^{-\mu}$ that approximates the fractional order calculus operator is designed from equation (35) above.

3.2. Numerical implementation of fractional order PID controller

The FOPID controller in the experimental control circuit needs to be designed using a discretized fractional order PID formulation, and in this paper, we use the Grünwald-Letnikov formulation, whose differential definition is shown in equation (2). The control law of fractional order PID is shown in the following equation [22-24].

$$u(t) = K_p e(t) + K_i \cdot {}_{t_0}D_t^{-\lambda} \mathrm{e}(t) + K_d \cdot {}_{t_0}D_t^{\mu} \mathrm{e}(t) \tag{23}$$

Preprints (www.preprints.org) | NOT PEER-REVIEWED | Posted: 17 January 2024 doi:10.20944/preprints202401.1302.v1

where ${}_{t_0}D_t^{-\lambda}$ and ${}_{t_0}D_t^{\mu}$ are fractional order calculus operators, where λ and μ must be real numbers, t is the independent variable, and t_0 is the lower bound of the variable, where the independent variable t is time. The uniform fractional order calculus operator ${}_{t_0}D_t^{\alpha}$ is defined as:

$$ {}_{t_0}D_t^{\alpha} f(t) = \begin{cases} \int_{t_0}^{t} f(\tau) d\tau^{-\alpha}, \alpha < 0 \\ f(t), \alpha = 0 \\ \dfrac{d^{\alpha}}{dt^{\alpha}} f(t), \alpha > 0 \end{cases} \tag{24} $$

where α is the fractional order.

The conjunction (2), (23) gives:

$$ u(t) = K_p e(t) + K_i \lim_{h \to 0} \frac{1}{h^{-\lambda}} \sum_{j=0}^{[(t-t_0)/h]} c_j e(t - jh) + K_d \lim_{h \to 0} \frac{1}{h^{\mu}} \sum_{j=0}^{[(t-t_0)/h]} d_j e(t - jh), (\lambda, \mu > 0) \tag{25} $$

where c_j and d_j are the integral term coefficients and differential term coefficients, respectively. The fractional order calculus equation is generally implemented by numerical approximation. The two coefficients can be approximated by using the following recursive equations.

$$ c_j = [1 - (1 - \lambda) / j] c_{j-1}, c_0 = 1, j = 1, 2, 3 \cdots \tag{26} $$

$$ d_j = [1 - (1 + \mu) / j] d_{j-1}, d_0 = 1, j = 1, 2, 3 \cdots \tag{27} $$

When the calculation step h chosen in the above equation is small enough, the limit finding operation in the above equation can be ignored, and t_0=0 in this paper, the following equation is obtained.

$$ u(t) = K_p e(t) + K_i h^{\lambda} \sum_{j=0}^{[t/h]} c_j e(t - jh) + K_d h^{-\mu} \sum_{j=0}^{[t/h]} d_j e(t - jh), (\lambda, \mu > 0) \tag{28} $$

From the above equation, the discretization equation for fractional order PID can be obtained as follows.

$$ u_k = K_p e_k + K_i h^{\lambda} \sum_{j=0}^{k} c_j e_{k-j} + K_d h^{-\mu} \sum_{j=0}^{k} d_j e_{k-j}, (\lambda, \mu > 0), (k = 1, 2, 3 \cdots) \tag{29} $$

To describe the fractional order PID control circuit more clearly, the flow of fractional order PID position control is described in Algorithm 1.

Algorithm 1. Fractional order PID position control flow.

Fractional order PID position control algorithm

Input: Control circuit controller parameters k_p, k_i, k_d, λ, μ ideal angle of rotation θ_0.

Output: actual rotation angle θ.

Preprints (www.preprints.org) | NOT PEER-REVIEWED | Posted: 17 January 2024 doi:10.20944/preprints202401.1302.v1

For (j=0; j<k; j++); do

Calculate the error between the target value and the actual value: $e_k=\theta_0-\theta$.

Calculate the binomial coefficients c_j and d_j from equations (26), and (27).

From equation (29) calculate the voltage of the input motor U.

Error transfer: $e_{k-j-1} = e_{k-j}$.

Return θ.

3.3. Judgment condition of damping adjustment

In this paper, the pavement unevenness of the input pavement excitation is mainly used as the basis for judging the damping adjustment. The classification criteria of known pavement unevenness are shown in Table 2.

Table 2. Road surface unevenness classification standards.

Pavement grade	$G_0(n_0)/10^{-6}\mathrm{m}^3$		
	Lower limit	Geometric mean	Upper limit
A	8	16	32
B	32	64	128
C	128	256	512

According to the data in table 2, the judgment basis for designing the damping adjustment is shown in the following equation.

$$c_s = b \cdot c = \begin{cases} \dfrac{9i\theta_{[q(G_1)]} + 2\pi}{2\pi} \cdot c, 8 \le G_0 \le 32 \\ \dfrac{9i\theta_{[q(G_2)]} + 2\pi}{2\pi} \cdot c, 32 < G_0 < 128 \\ \dfrac{9i\theta_{[q(G_3)]} + 2\pi}{2\pi} \cdot c, 128 < G_0 < 512 \end{cases} \quad (30)$$

According to equation (30), the total damping coefficient c_s of the suspension system is the optimal damping coefficient obtained by parameter search when the road surface unevenness is G_1, which corresponds to level A of the road surface. For the road surface unevenness G_2, the total damping coefficient c_s of the suspension system is the best damping coefficient obtained by parameter optimization, which corresponds to level B of the road surface. In case of G_3, the total damping coefficient $c_s$is the best damping coefficient obtained by parameter optimization, which corresponds to the suspension system at level C. The damping coefficient c_s is the best damping coefficient obtained by parameter optimization. This means that the damping coefficient can be flexibly adjusted according to changes in road leveling, enabling the suspension system to achieve better damping in all road conditions.

3.4.Objective function and constraints

Before determining the parameters to be searched, the objective function of the search and the constraints to be satisfied by the search results need to be specified. Suspension system performance is evaluated based on body acceleration, suspension dynamic deflection, and tire dynamic loads, which interact with each other. Body acceleration is used to evaluate ride smoothness, tire dynamic loads are used to evaluate handling stability, and suspension dynamic deflection measures the effect on body attitude. Therefore, when performing active suspension control, handling stability needs to be taken into account and the suspension dynamic deflection needs to be controlled within an

Preprints (www.preprints.org) | NOT PEER-REVIEWED | Posted: 17 January 2024 doi:10.20944/preprints202401.1302.v1

acceptable range based on optimizing the vehicle ride smoothness. Therefore, the objective function J_1 is constructed as shown below.

$$J_1 = \rho_1 \frac{rms(\ddot{x}_2)}{rms(\ddot{x}_2)_p} + \rho_2 \frac{rms(x_2 - x_1)}{rms(x_2 - x_1)_p} + \rho_3 \frac{rms[k_1(x_1 - q)]}{rms[k_1(x_1 - q)]_p} \tag{31}$$

Meet the constraints:

$$s.t. = \begin{cases} \dfrac{rms(\ddot{x}_2)}{rms(\ddot{x}_2)_p} < 1 \\ x_2 - x_1 < b_1 \\ \dfrac{rms[k_1(x_1 - q)]}{rms[k_1(x_1 - q)]_p} \le 1 \end{cases} \tag{32}$$

where the subscript p represents the passive suspension indicators and rms(.) denotes the root mean square value of each indicator. The purpose of this design is to dimensionlessize each performance index and facilitate the selection of weighting factors. ρ_1, ρ_2 and ρ_3 are the weighting coefficients due to the different importance of each index in the suspension system. Let $\sum_{i=1}^{3} \rho_i = 1$and determine the weighting coefficient of the required optimization indexes according to the required order of optimization of each index combined with the constraints. Since the permitted travel of the oil and gas damper is 0.04m in the equiproportional model used in the experiment, $b_1 = 0.04$ is taken in the constraint. When the output of the suspension system does not satisfy the constraint, the weighting coefficients ρ_1, ρ_2 and ρ_3 to be readjusted.

3.5.Parametric optimization principle and process

In this paper, the particle swarm algorithm [25] is used to find the optimal objective function J_1 and the goal is to find the optimal turning angle θ_0, to achieve the optimal control of body acceleration and improve the smoothness of the vehicle. The principle of the particle swarm algorithm for finding the optimum is shown below:

The initial parameters of the particle swarm are set, including the inertia factor w, acceleration constants o_1 and o_2, the number of particles in the swarm S, the maximum number of particle iterations T, the upper bound U_B and the lower bound U_L for the parameter search. The position information of particle m is $X_m(x_{m1},\ldots, x_{mn})$. The particle search velocity is $V_m(v_{m1},\ldots,v_{mn})$, n is the number of optimization-seeking parameters, i.e., the dimension of the solution space, and n=1 when the optimization is sought for the objective function J_1. To prevent the particle velocity from being too large and exceeding the set boundary, the velocity of particle m is limited to $-v_{max} \le v_{mn} \le v_{max}$, the part exceeding is taken as the boundary value.

t denotes the number of current iterations of the particle and the particle velocity update formula is shown in the following equations.

$$H(t) = wv_{mn}(t) + o_1 \cdot r_1 \cdot [pbest_{mn}(t) - x_{mn}(t)] + o_2 \cdot r_2 \cdot [gbest_n(t) - x_{mn}(t)] \tag{33}$$

$$v_{mn}(t+1) = \begin{cases} H(t), -v_{\max} \le H(t) \le v_{\max} \\ v_{\max}, H(t) > v_{\max} \\ -v_{\max}, H(t) < v_{\max} \end{cases} \tag{34}$$

The particle position update formula is shown in the following equation.

Preprints (www.preprints.org) | NOT PEER-REVIEWED | Posted: 17 January 2024 doi:10.20944/preprints202401.1302.v1

$$x_{mn}(t+1) = x_{mn}(t) + v_{mn}(t+1) \tag{35}$$

Where $pbest_{mn}(t)$ denotes the particle m individual current optimal position parameter and $gbest_n(t)$ denotes the particle swarm global current optimal position parameter. r_1、r_2 denote the random number between [0,1].

The individual m optimal position update equation is:

$$\text{p}best_m = \begin{cases} pbest_m(t), J[X_m(t+1)] \geq J[pbest_m(t)] \\ X_m(t+1), J[X_m(t+1)] < J[pbest_m(t)] \end{cases} \tag{36}$$

The global optimal position update formula is:

$$J[gbest(t)] = \min\left\{J[pbest_1(t)], \cdots, J[pbest_S(t)]\right\} \tag{37}$$

When the objective function J_1 is optimized, the upper bound U_B is set to $[2\pi/i]$ and the lower bound U_L is set to [0], because the maximum rotation angle of the adjustable damping knob is 2π. The rest of the initial parameters are shown in Table 3. The algorithm optimization flow is shown in Figure 8.

Table 3. Initial parameters of the particle swarm algorithm.

Parameters	value
w	1
o_2	0.5
T	100
o_1	0.5
S	10
v_{max}	10

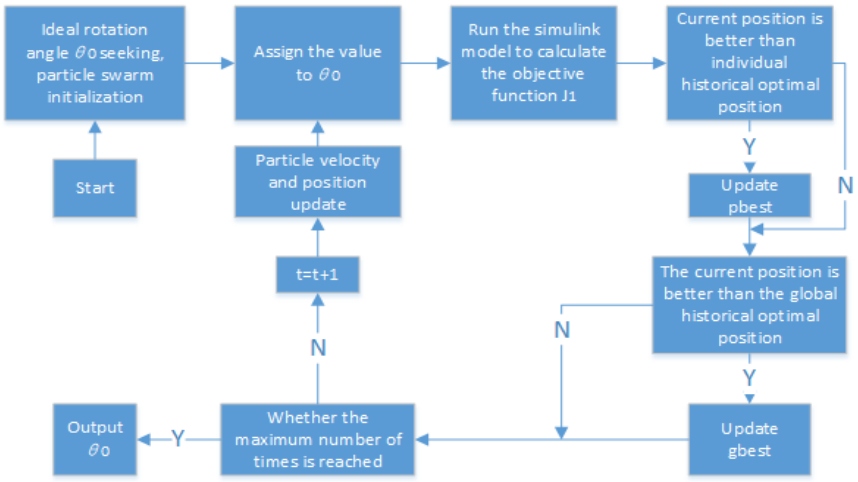

Figure 8. Suspension system parameter optimization flow chart.

After preliminary simulations and experimental studies, combined with the actual parameters of the experimental rig, the values of each parameter can be obtained as shown in Table 4 below.

Table 4. Suspension system parameter table.

Parameters	value	Parameters	value
m_1/kg	0.4	$k_1/N{\cdot}m^{-1}$	1680
m_2/kg	2.7	$k_2/N{\cdot}m^{-1}$	155
e	3	$c/N{\cdot}s{\cdot}m^{-1}$	8

Preprints (www.preprints.org) | NOT PEER-REVIEWED | Posted: 17 January 2024 doi:10.20944/preprints202401.1302.v1

p	0.85	i	1/20
ρ_1	0.5	r/Ω	14.4
ρ_2	0.2	ρ_3	0.3
L/H	0.3	$J/kg{\cdot}m^2$	0.02

Among them, the selection of the reduction ratio i of the reducer mainly considers the following factors:

As mentioned earlier, if the reduction ratio of the selected reducer is too large, the output torque may not be sufficient to push the damping adjustment knob, resulting in a decrease in control accuracy. Conversely, if the reduction ratio is too small, this will cause the time required for damping adjustment to increase to a given value, thereby slowing down the response of the system. Therefore, the reduction ratio i=1:20 is selected to balance the system performance, taking into account the control accuracy and output torque, while referring to the available reducer models on the market.

The simulation model of the suspension system is established according to the parameters in Table 4, and then the objective function J_1 and the ideal turning angle θ_0 are searched for under each road level respectively, and the searched results are shown in Figure 9 below.

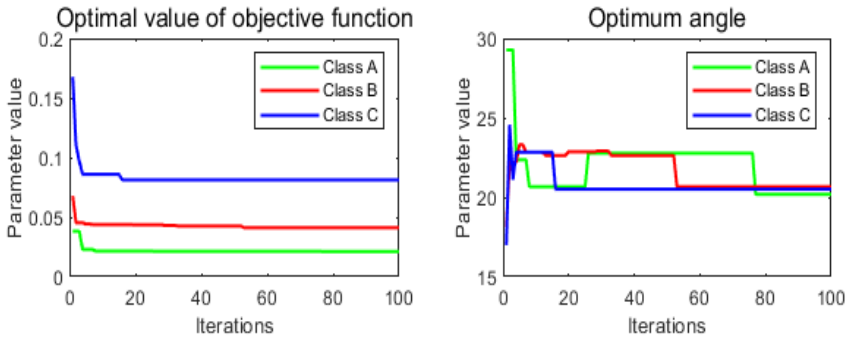

Figure 9. Parametric optimization search results chart.

From the Figure 9, it can be seen that the optimal values of the objective function J_1 gradually increase with the increase of the pavement grade, which are 0.0211, 0.0453 and 0.0813, respectively. while the optimal values of the ideal turning angle first increase and then decrease, which are 20.1804, 20.6578, and 20.5130 respectively.After determining the optimal value of the ideal angle, the optimal angle value obtained from the optimization search is used as the given value of the controller, and the PID algorithm and the fractional-order PID algorithm are used to control the motor angle respectively and the control principle is shown in Fig.7. After a large number of simulations and experimental trials, the controllerparameters are obtained as shown in Table 5 below.

Table 5. Controller parameter selection.

Control algorithms	Parameter				
	K_p	K_i	K_d	λ	μ
PID	10	1	10	1	1
FOPID	11	1	15	0.8	0.9

4. Simulation and experimental results study analysis

To verify the accuracy of the established fractional order nonlinear suspension system describing the oil-pneumatic suspension, the superiority of the fractional order PID controller compared with the PID controller, and the feasibility of the designed electric oil-pneumatic active suspension, simulations, and bench tests are performed for the equiproportional electric oil-pneumatic active suspension device shown in Figure 10.

Preprints (www.preprints.org) | NOT PEER-REVIEWED | Posted: 17 January 2024 doi:10.20944/preprints202401.1302.v1

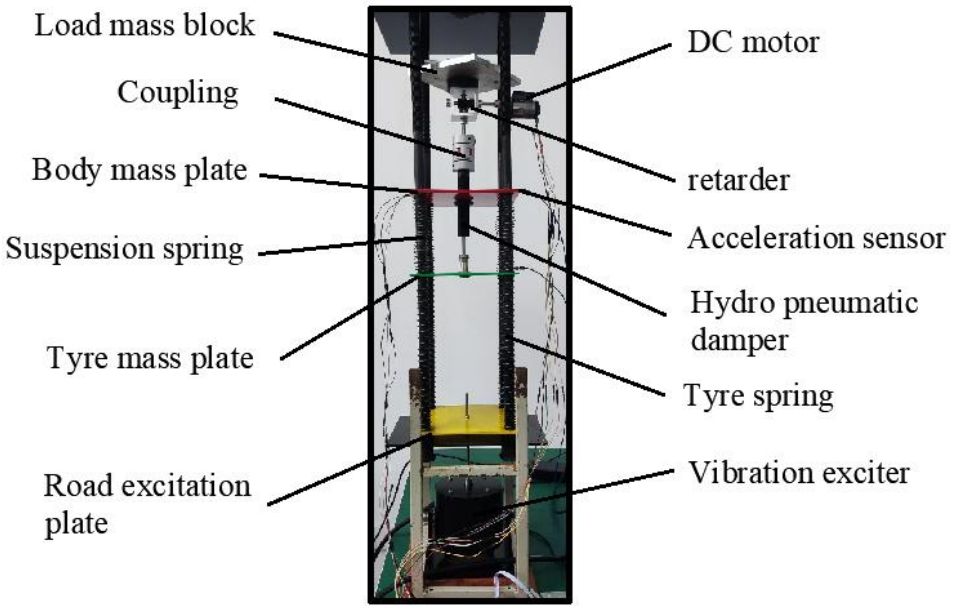

Figure 10. Equivalent proportional oil-pneumatic suspension equipment.

4.1. Study on the superiority of fractional order nonlinear passive suspension model

Before proceeding to the active suspension control study, the accuracy of the used fractional order nonlinear passive suspension model is demonstrated. At this point, b=1, the body acceleration, suspension dynamic deflection, and tire dynamic load under simulation and test are obtained as shown in Figures 11 and 12 below.

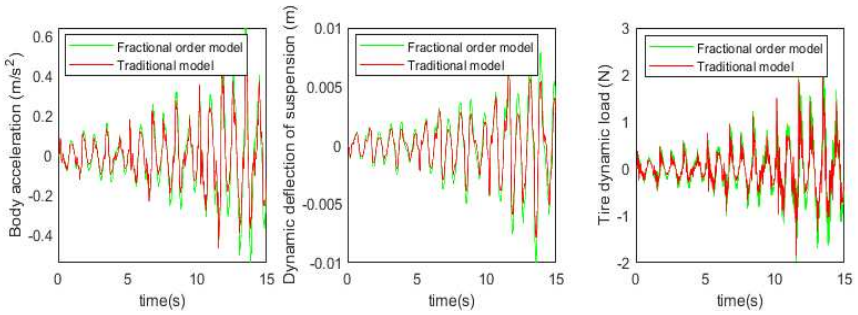

Figure 11. Passive suspension model simulation results.

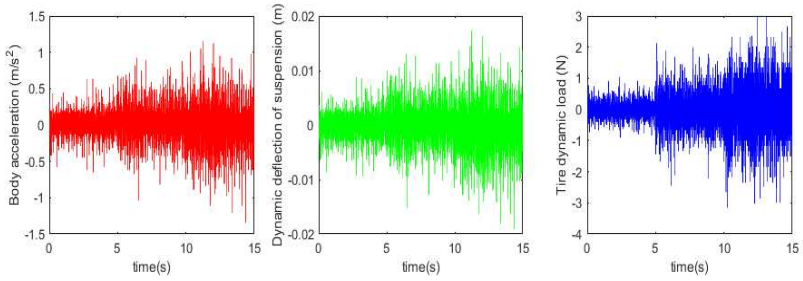

Figure 12. Passive suspension model test results.

Based on the simulation and test results, the root mean square values of each suspension index were obtained as shown in Table 6 below.

Table 6. Root mean square values of performance indicators.

Performance Indicators	Numerical access

Preprints (www.preprints.org) | NOT PEER-REVIEWED | Posted: 17 January 2024 doi:10.20944/preprints202401.1302.v1

	Test	Traditional Model Simulation	Difference from test	Fractional order model simulation	Difference from test
Body acceleration /$m{\cdot}s^{-2}$	0.2095	0.1427	31.9%	0.1814	13.4%
dynamic deflection /m	0.0030	0.0022	26.7%	0.0028	6.7%
Tire dynamic load /N	0.5646	0.4215	25.3%	0.5326	5.7%

It can be observed from the data in the above figure and table that the simulation results of the fractional-order nonlinear suspension system model used in this paper are closer to the actual values compared to the conventional nonlinear suspension system model. Specifically, the accuracy of body acceleration is improved by 18.5%, the accuracy of suspension dynamic deflection is improved by 20%, and the accuracy of tire dynamic load is improved by 19.6%. It can be seen that the use of a fractional order nonlinear suspension system model to simulate the oil and gas suspension system can reflect the actual situation more accurately than the traditional nonlinear model.

4.2. Fractional order PID controller superiority verification

To optimize motor corner control, this paper introduces the fractional-order PID control algorithm to replace the traditional PID control algorithm and verifies the excellent performance of the fractional-order PID control algorithm in motor corner control through simulation and test results. In the actual implementation, this paper chooses the STM32-F407 development board as the carrier of the control algorithm and uses Keil software to write PID and fractional-order PID control programs in the upper computer and set the initial parameters of the controller. The control driver board is powered by a transformer, which drives the motor through an encoder. The Hall sensor on the driver board is responsible for acquiring the position signal of the motor and feeding it back to the development board. The development board then controls the angle of the motor in real-time and feeds the control results to the host computer for display Figure 13 shows the information about the test equipment and the test flow.

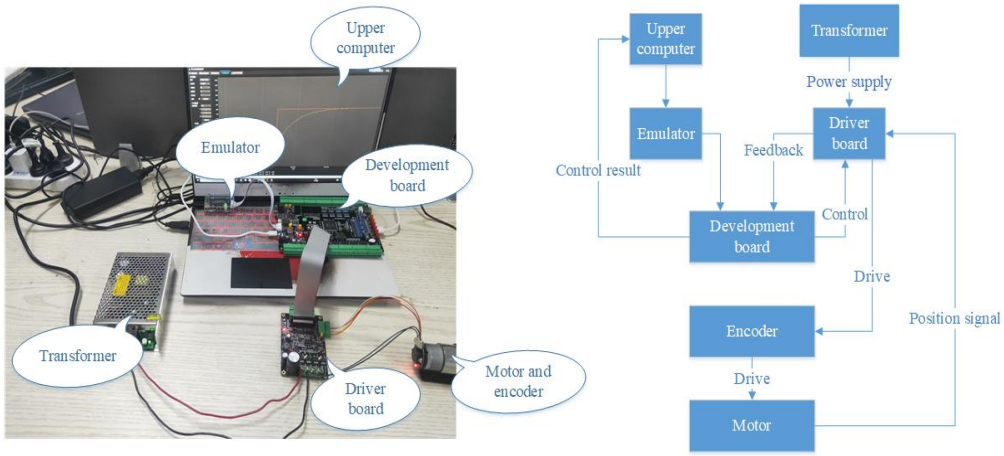

Figure 13. Motor angle control test bench and control flow.

To avoid system instability caused by excessive overshoot, the initial rotation angle is set to 20 rad. The simulation and test results are shown in Figure 14 below.

Preprints (www.preprints.org) | NOT PEER-REVIEWED | Posted: 17 January 2024 doi:10.20944/preprints202401.1302.v1

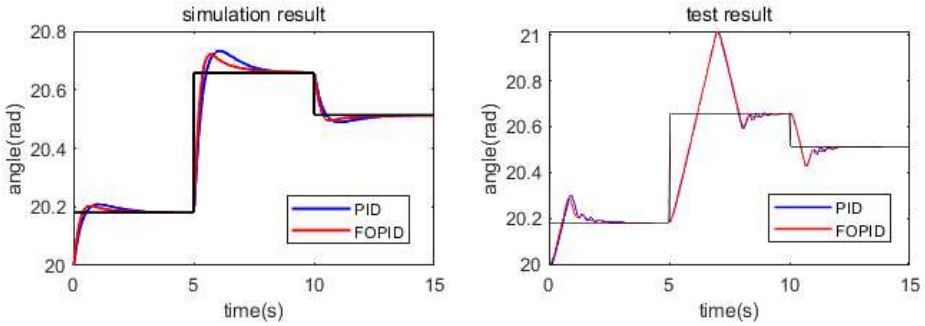

Figure 14. Motor angle control results.

It can be observed from the simulation and experimental results that the fractional order PID controller shows more effective optimization in motor corner control compared to the conventional PID controller. In the simulation, the root mean square value of deviation under PID control is 0.2629, while the root mean square value of deviation under fractional-order PID control is 0.2563. In addition, the root mean square value of deviation under PID control is 0.1158, while the root mean square value of deviation under fractional-order PID control is 0.1147. This suggests that the use of fractional-orderPID controllers can improve the overall performance of the motor corner control while reducing the deviation. overall performance of the corner control.

4.3. Suspension active control results analysis

To verify the feasibility of the designed fractional-order PID position feedback control in an electric-hydrocarbon active suspension system, the body acceleration, suspensiondynamic deflection, and tire dynamic loads in the passive and active control states were simulated and experimentally investigated. The constructed test rig for the active suspension system is shown in Figure 15 below. This study aims to evaluate the performance of fractional-order PID control in a real active suspension system to gain a more comprehensive understanding of its potential for improving vehicle dynamic characteristics.

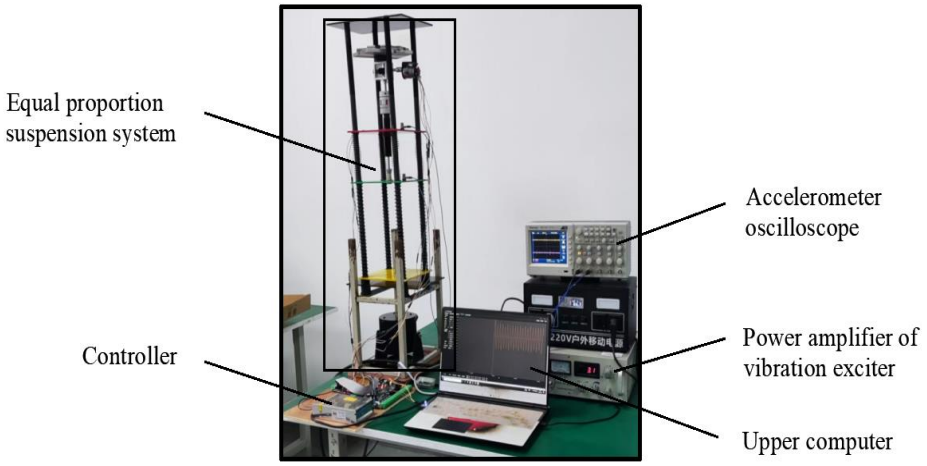

Figure 15. Suspension system test bench.

The simulation and experimental results are shown in Figures 16 and Fiure 17 below.

Preprints (www.preprints.org) | NOT PEER-REVIEWED | Posted: 17 January 2024 doi:10.20944/preprints202401.1302.v1

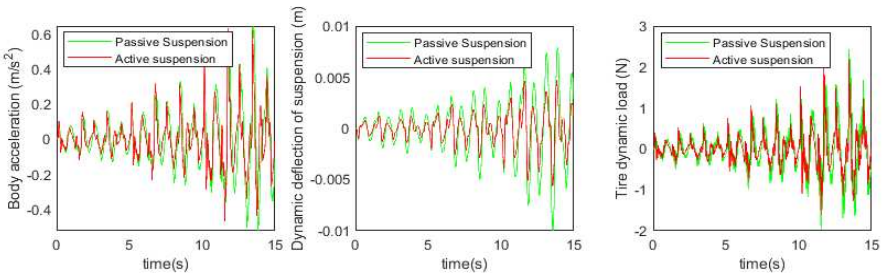

Figure 16. Active and Passive Suspension Simulation Results.

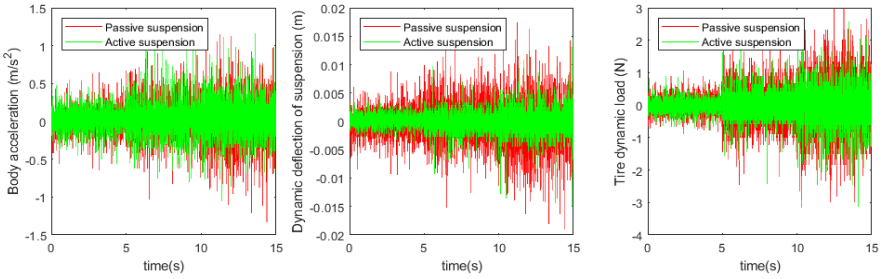

Figure 17. Active and Passive Suspension Test Results.

Based on the simulation and test results, the root mean square values of each suspension index were obtained as shown in Table 7 below.

Table 7. Root mean square values of performance indicators.

Performance Indicators	Numerical access			
	Passive Suspension Simulation	Active Suspension Simulation	Passive Suspension Experiment	Active Suspension Experiment
Body acceleration /$m{\cdot}s^{-2}$	0.1814	0.1384	0.2095	0.1882
dynamic deflection /m	0.0028	0.0016	0.0030	0.0017
Tire dynamic load /N	0.5326	0.4025	0.5646	0.4142

According to the simulation results, compared with the passive suspension system, the electric oil-air active suspension achieves 75.2% optimization in body acceleration, 57.1% optimization in suspension dynamic deflection, and 75.6% improvement in tire dynamic load. The experimental validation shows that compared with the traditional passive oil-air suspension system, the designed electric oil-air active suspension can effectively improve the damping performance of the suspension system, which is theoretically feasible. The specific experimental results show that the body acceleration is increased by 89.8%, the suspension dynamic deflection is increased by 56.7%, and the tire dynamic load is increased by 73.4%. This indicates that the electric oil-pneumatic active suspension system has been significantly optimized in terms of body acceleration, suspension dynamic deflection, and tire dynamic load, which verifies the accuracy of the simulation conclusions and confirms the feasibility of the designed structure for engineering applications.

5. Conclusion

This study focuses on an electric-hydrocarbon active suspension under fractional-order PID position feedback control and constructs a fractional-order nonlinear system model describing this suspension type. We developed mathematical models for each mechanism and conducted a series of in-depth studies through MATLAB and Simulink simulations as well as bench experiments. The main contributions of the research include:

Preprints (www.preprints.org) | NOT PEER-REVIEWED | Posted: 17 January 2024 doi:10.20944/preprints202401.1302.v1

1)Using the particle swarm algorithm, the optimization of damping coefficients of the suspension system under different road surface grades is successfully achieved based on the road surface unevenness coefficient. This research provides an effective method to find the optimal damping coefficients.

2)Through the simulation and experiment of the fractional-order nonlinear oil-pneumatic suspension system, the data of body acceleration, suspension dynamic deflection, and tire dynamic deformation of the suspension system were obtained. This confirms that the fractional-order nonlinear oil-air suspension system is more suitable for describing the dynamic characteristics of oil-air suspensions than the conventional nonlinear system.

3)A digital implementation of a fractional-order PID control circuit for motor angle control is proposed. The superiority of the fractional order PID control circuit over the conventional PID control circuit is verified through simulation and experimentation of the actuator control circuit.

4)An actuator structure is designed to adjust the damping using a motor, and the feasibility of this design is proved through simulation and experiment. This actuator structure effectively realizes the damping adjustment of the suspension system, so that the performance index of the active suspension system is better than that of the passive suspension system.

Author Contributions: Conceptualization, Yaozeng Hu and Jiang Liu; Funding acquisition, Jiang Liu; Methodology, Jianze Liu, Jingming Zhang and Wang Zhuang; Project administration, Jiang Liu; Software, Jingming Zhang and Yaozeng Hu; Visualization, Jianze Liu and Jiang Liu; Writing – original draft, Yaozeng Hu, Jianze Liu and Wang Zhuang; Writing – review & editing, Jianze Liu, Yaozeng Hu and Wang Zhuang.

Acknowledgments: This research was funded by the Natural Science Foundation of Shandong Province (ZR202111180079). The authors gratefully acknowledge the supporting agency.

Institutional Review Board Statement: Not applicable.

Informed Consent Statement: Not applicable.

Data Availability Statement: Not applicable.

Declaration of Conflicting Interests: The authors declared no potential conflicts of interest concerning the research, authorship, and/or publication of this article.

References

1. Ezeta, J.H.; Mandow, A.; Cerezo, A.G. Active and Semi-active Suspension Systems: A Review. *Revista iberoamericana de automatica e informatica industrial*. **2013**, *10*, 121-132. 10.1016/j.riai.2013.03.002.
2. Tseng, H.E.; Hrovat, D. State of the art survey: active and semi-active suspension control. *Vehicle system dynamics*. **2015**, *53*, 1034-1062. 10.1080/00423114.2015.1037313.
3. Palanisamy, S.; Karuppan, S. Fuzzy control of active suspension system. *journal of vibroengineering*. **2016**, *18*, 3197-3204. 10.21595/jve.2016.16699.
4. Basargan, H.; Mihaly, A.; Gaspar, P.; Sename, O. Adaptive Semi-Active Suspension and Cruise Control through LPV Technique. *Applied sciences-basel*. **2021**, *11*, 290. 10.3390/app11010290.
5. Zapateiro, M.; Pozo, F.; Karimi, H.R.; Luo, N.S. Semiactive Control Methodologies for Suspension Control With Magnetorheological Dampers. *IEEE-ASME transactions on mechatronics*. **2012**, *17*, 370-380. 10.1109/TMECH.2011.2107331.
6. Dou, G.W.; Yu, W.H.; Li, Z.X.; Khajepour, A.; Tan, S.Q. Sliding Mode Control of Laterally Interconnected Air Suspensions. *Applied sciences-basel*. **2020**, *10*, 4320. 10.3390/app10124320.
7. Kwon, K.; Seo, M.; Kim, H.; Lee, T.H.; Lee, J.; Min, S. Multi-objective optimisation of hydro-pneumatic suspension with gas-oil emulsion for heavy-duty vehicles. *Vehicle system dynamics*. **2019**, *58*, 1146-1165. 10.1080/00423114.2019.1609050.
8. You, H.; Shen, Y.J.; Yang, S.P. Optimization design of passive fractional suspension parameters based on particle swarm optimization algorithm. *Journal of vibration and shock*. **2017**, *36*, 224-228+254. http://jvs.sjtu.edu.cn/CN/Y2017/V36/I16/224.
9. Chang, Y.J.; Tian, W.W.; Jin, G.E. Active Control of Nonlinear Fractional Suspension Based on Differential Geometry Method. *Journal of Vibration and Shock*. **2021**, *40*, 270-276. http://jvs.sjtu.edu.cn/CN/Y2021/V40/I4/270.

Preprints (www.preprints.org) | NOT PEER-REVIEWED | Posted: 17 January 2024 doi:10.20944/preprints202401.1302.v1

10. Ahamed, R.; Rashid, M.M.; Ferdaus, M.M. et al. Design and modeling of energy generated magneto rheological damper. *Korea-australia rheology journal*. **2016**, *28*, 67–74. https://doi.org/10.1007/s13367-016-0007-6.
11. Park, H.G.; Jeong, K.H.; Park, M.K.; Ahn, K.K. Electro Hydrostatic Actuator System Based on Active Stabilizer System for Vehicular Suspension Systems. *International journal of precision engineering and manufacturing*. **2018**, *19*, 993-1001. 10.1007/s12541-018-0117-9.
12. Pakdelian, S. A compact and light-weight generator for backpack energy harvesting. *2016 IEEE Energy Conversion Congress and Exposition (ECCE)*, **2016**, 1-8. 10.1109/ECCE.2016.7854658.
13. George, R.; Huard, P. A. Regenerative Suspension System. *U.S. Patent*. **2005**, 20060016629.
14. Zhao, Z.H.; Guan, Y.L.; Chen, S.A.; Experimental Research on PMSM Ball Screw Actuator and Structural Design Suggestion of Featured Active Suspension. *IEEE access*. **2020**, *8*, 66163-66177. 10.1109/ACCESS.2020.2985118.
15. Podlubny I. An Introduction to Fractional Derivatives, Fractional Differential Equations, to Methods of their Solution and some of their Applications. London: *Academic Press*. **1999.**
16. Sun, H.L.; Jin, C.; Zhang W.M.; Li H.; Tian H.Y. Modeling and experimental analysis of oil and gas suspensions based on fractional order calculus. *Vibration and Shock*. **2014**, *33*, 167-172+190. 10.13465/j.cnki.jvs.2014.17.030.
17. Cao, J.Y.; Ma, C.B.; Xie, H.; Jiang, Z.D. Nonlinear Dynamics of Duffing System with Fractional Order Damping. *Journal of computational and nonlinear dynamics*. **2010**, *5*,041012. 10.1115/1.4002092.
18. Scherer, R.; Kalla, S.L. Tang, Y.F.; Huang, J.F. The Grunwald-Letnikov method for fractional differential equations. *Computers & mathematics with applications.* **2011**, *62*, 902-917. 10.1016/j.camwa.2011.03.054.
19. Yang, H.; Liu, J.; Li, M.; Zhang, X.; Liu, J.; Zhao, Y. Adaptive Kalman Filter with L2 Feedback Control for Active Suspension Using a Novel 9-DOF Semi-Vehicle Model. *Actuators.* **2021**, *10*, 267. https://doi.org/10.3390/act10100267.
20. Mucka, P. Simulated Road Profiles According to ISO 8608 in Vibration Analysis. *Journal of testing and evaluation*. **2018**, *46*, 405-418. 10.1520/JTE20160265.
21. Xue, D.Y.; Zhao, C.N.; Chen, Y.Q. A modified approximation method of fractional order system. *Proceedings of IEEE Conference on Mechatronics and Automation*. **2006**,1043-1048.
22. Pritesh, S.; Sudhir, A. Review of fractional PID controller. Mechatronics. **2016**, *38*, 29-41. https://doi.org/10.1016/j.mechatronics.2016.06.005.
23. Axtell, M.; Bise, M.E. Fractional calculus application in control systems. *IEEE Conference on Aerospace and Electronics*. **1990**, *2*, 563-566. 10.1109/NAECON.1990.112826.
24. Hamamci, S.E. Stabilization using fractional-order PI and PID controllers. *Nonlinear Dynamics*. **2008**, *51*, 329 − 343. https://doi.org/10.1007/s11071-007-9214-5.
25. Martins, C.H.; Dos Santos, R.P.B.; Santos, F.L. Simplified particle swarm optimization algorithm. *Acta scientiarum-technology*. **2012**, *34*, 21-25. 10.4025/actascitechnol.v34i1.9679.

Disclaimer/Publisher's Note: The statements, opinions and data contained in all publications are solely those of the individual author(s) and contributor(s) and not of MDPI and/or the editor(s). MDPI and/or the editor(s) disclaim responsibility for any injury to people or property resulting from any ideas, methods, instructions or products referred to in the content.